A Novel Technique for Improved Measurement of Graphite and Inclusions in Ductile Iron Contaminated by Boron

Chase Schroeder,
Colleen Lehrer, Simon Lekakh, and Laura Bartlett
Missouri University of Science and Technology, Rolla, Missouri, USA

ABSTRACT

The highly heterogeneous microstructure of ductile iron in casting includes graphite particles, non-metallic inclusions, microporosity, and other features, such as carbides distributed in the ferrite/pearlite matrix. Determination and comprehensive quantification of microstructural features are practically important, however challenging. An advanced methodology based on an automated scanning electron microscopy/energy dispersive X-ray (SEM/EDX) analysis was developed and compared to the standard optical imaging method. In addition to backscattered electron contrast, sensitive to atomic number, a novel methodology added EDX data to identify and classify the multiple structural features at micron resolution thresholding. To quantify the shape of individual phases, eight chord raster algorithms were used and compared to standard metrology based on Feret diameter. A micropattern with regular shapes and the real microstructure of contaminated ductile iron in section sizes from 5 to 30 mm were used for comparative studies. The advantages of this novel methodology were statistically compared.

Keywords: microstructure, cast iron, graphite shape, nodularity, automated scanning electron microscopy/energy dispersive X-ray, SEM/EDX

INTRODUCTION

The microstructure of ductile iron contains graphite particles of varying nodularity, non-metallic inclusions, microporosity, and in some cases, carbides. All of these features have varying effects on the mechanical properties of ductile iron; however, they are not easily distinguished from one another using standard optical metallographic techniques. For example, the effects of these features on the mechanical properties of cast irons at low, medium and high temperatures and corrosion and oxidation resistances have recently been investigated and summarized.[1] It was shown that graphite shape is the dominating factor in controlling strength and ductility,[2] while carbide increases hardness,[3] and a certain low level of microporosity is critical for mechanical properties (ductility and strength) of the casting.[4] The multiple negative effects of non-metallic inclusions on steel properties are well documented;[5] however, considering their critical role in heterogeneous nucleation of graphite phases,[6-8] a controlled level of targeted non-metallic inclusions improves graphite nucleation nodule count. At the same time, clustering, flotation in the mold, and segregation of non-metallics during solidification have negative effects on spheroidal graphite iron (SGI) properties.[9] It would be beneficial for foundries to understand the role of inclusion chemistry and distribution on both graphite nucleation potential and corresponding mechanical properties. However, standard optical metallography cannot accurately distinguish inclusions from other features in the matrix iron and chemical analysis is not possible.

All of these indicate the practical importance of determination and comprehensive quantification of the family of structural features in cast irons. Considering possible micro- and macro- heterogeneity of the structure formed during solidification of complicated shape castings, it is very important to obtain statistically significant results, therefore different types of quantitative methods have been developed.[10-11] Table 1 illustrates the capabilities and comparison of traditional metallography to several novel methodologies, such as an automated SEM/EDX analysis and 3D-micro tomography.[12] An automated SEM/EDX analysis provided a significant step forward to compare optical metallography in qualitative methodology of determination of a chemical nature of microstructural features and obtained better resolution when compared to both optical and micro-computed tomography (micro-CT) methods. The specific details of the application of an automated SEM/EDX method to qualify and quantify the heterogenous microstructure of SGI with spherical graphite are described in this paper.

Table 1. Comparison of Capabilities of Methods used for SGI Casting Quality Analysis

Method	Resolution, microns	Graphite shape	Nodule number	Graphite volume	Spatial distribution	Non-metallic inclusions	Micporosity	Cost/ time
Optical	>10	2D	2D	By reconstruction	2D	No	Yes	Low
Automated SEM/EDX	>1	2D	2D	By reconstruction	2D	Yes	Yes	High
Micro-CT	>3	3D	3D	Yes	3D	No	Yes	Very high

Among several important quantitative characteristics of the different populations of microconstituents (graphite, inclusions, pores, etc.) such as the area/volume and number per unit area, the shape parameter is more controversial and difficult to quantify.

Several standards suggest methods for characterization of graphite shape and distribution into several classes,[13] however, departure from the ideal have been discussed in recent publications.[14-16]

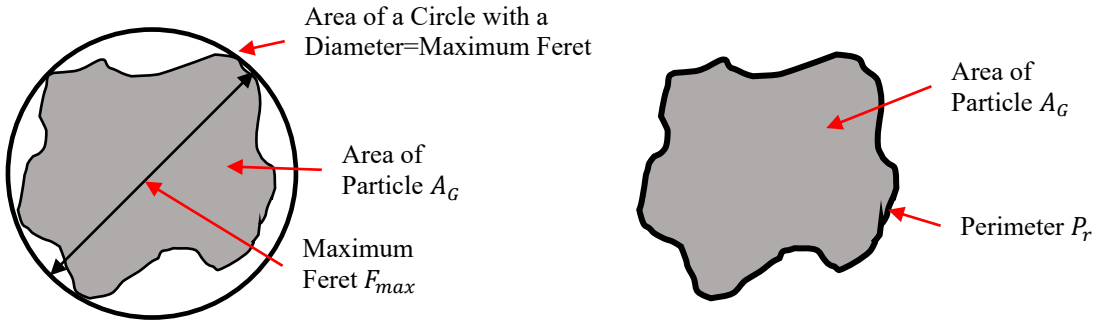

Figure 1. Schematic representation of roundness shape factor & sphericity shape factor. (Image redrawn from Ref. 1.)

$$\text{Roundness Shape Factor: } (RSF) = 4A_G/\pi F_{max}^2 \qquad \text{Eqn. 1}$$

$$\text{Sphericity Shape Factor: } (SSF) = 4\pi A_G/P_r^2 \qquad \text{Eqn. 2}$$

Figure 1 illustrates two common methods which are used to quantify graphite nodule shape. The first method is based on circumferential or external Feret diameter (F_{max}) for calculating Roundness Shape Factor (RSF) using Eqn. 1 and considering the graphite area (A_G) The second method determines Sphericity Shape Factor (SSF) from the measured particle perimeter P_r (Eqn. 2). shape. These two methods have advantages and disadvantages when applied for actual graphite shape quantification. The RSF method, which is based on the Feret diameter, does not consider micro-roughness or concave type shape distortions. It could be concluded that the SSF method, which is based on the actual perimeter, is better suited for graphite shape determination.[17] However, this is a hypothetical conclusion for an ideal and infinity small pixel size relative to the dimensions of measured structural features. In practice, the typical micron range of optical image resolution will significantly affect a measured perimeter of 2–50-micron graphite particles. For example, several tests were performed using high-resolution digital images of figures with smooth, without micro-roughness perimeters, including an oval (Fig. 2a), a square (Fig. 2b) and distorted convex-concave shapes (Fig. 2c). These shapes were rotated and scaled down in digital images to verify the stability of measured RSF and SSF parameters with commercial ImageJ software.[17] It was determined that the measured values for the same shape depended on rotational angle and size/pixel ratio (see error data in Fig. 2). The SSF method, which is based on measured perimeter, provided significantly larger errors for sharp (square vs. oval) and irregular shapes. ImageJ and other image analysis software use chessboard type XY pixel meshing and special methods to determine the length of the boundary crossing several pixels; however, it was challenging to achieve a resulting perimeter without integrated error. For example, for irregular shaped graphite particles, such as shown in Fig. 2c, the SSF method showed twice as large of an error than the RSF method. At the same time SSF gives a larger value of shape factor than the RSF method based on Feret diameter.

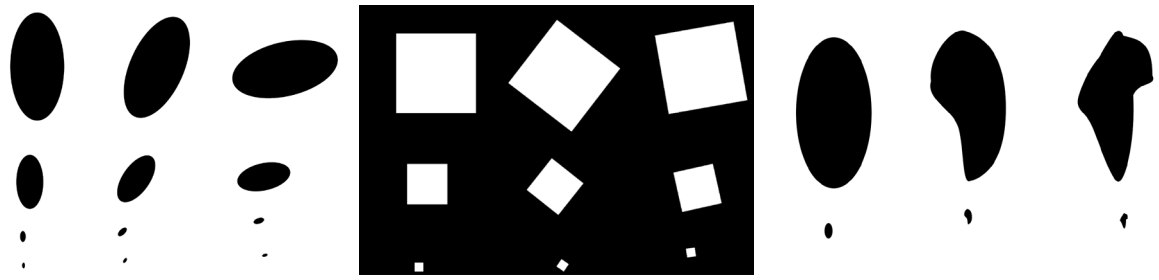

RSF	0.2%	0.7%	2-5%
SSF1	0.5%	5%	5-10%
	(a)	***(b)***	***(c)***

Figure 2. ImageJ measurement % error for different shapes at varied sizes and orientations: (a) oval, (b) rectangular and (c) irregular convex and concaved.

The goal of this study was to overturn the disadvantages of optical image analysis in detecting targeting phases (graphite vs. inclusions or pores) and eliminate uncertainties in quantification of graphite particle shape by using an automated SEM/EDX analysis. Significantly higher resolution, when compared to optical imaging, was utilized in the special algorithm for measuring particle shape, based on end-connected 8 chord raster. To illustrate the high sensitivity of the suggested method, step block castings were analyzed from laboratory-melted SGI with varying nodularity, controlled by differences in boron contamination.

METHODOLOGY

The principal of the application of automated SEM/EDX analysis of microstructural features in iron based alloys, including steel and cast iron were described in Ref. 18. Backscattered electron (BSE) imaging, which produces contrast that is related to atomic number, was utilized to distinguish graphite, non-metallic inclusions and pores from the lighter contrast iron matrix (Fig. 3). The line scan illustrates a signal intensity and used thresholding for graphite (green zone) by avoiding upper/lower signal saturation and considering signal noise. Optimal magnification was used to have more than ten nodules (minimum magnification) in the field view and avoiding more than 5% nodules at boundary located (maximum) magnification. The SEM analysis has several image quality parameters and more sophisticated settings when compared to optical imaging, including step size, beam diameter and others. The effects of setting parameters on measured particle number, size and area were discussed by Harris et al.[19] and optimal settings were used considering dimensions of the main feature of interest, which was the graphite. In this study, the 2 – 100-micron feature dimension threshold was utilized.

The automated SEM/EDX methodology utilizes two modes: first, search mode had described above setting to detect contrast of a targeted feature, after which detailed geometrical morphology and phase composition were determined in the analysis mode. To do the analysis, the system, after detecting the feature of interest from contrast, automatically increases magnification for geometrical measurements using several methods. It automatically determines the center of mass of each particle and collects the EDX spectrum, which was used to classify features of interest by chemistry. The measuring mode also had several specific settings which were developed for SGI analysis. The first one is related to shape measuring. In this study, parameters such as maximum Feret diameter and perimeter were determined, similar to what was utilized by ImageJ for optical analysis. The perimeter was determined from the length of segments connected to the ends of 8 chords raster from the center of mass (Fig. 4).

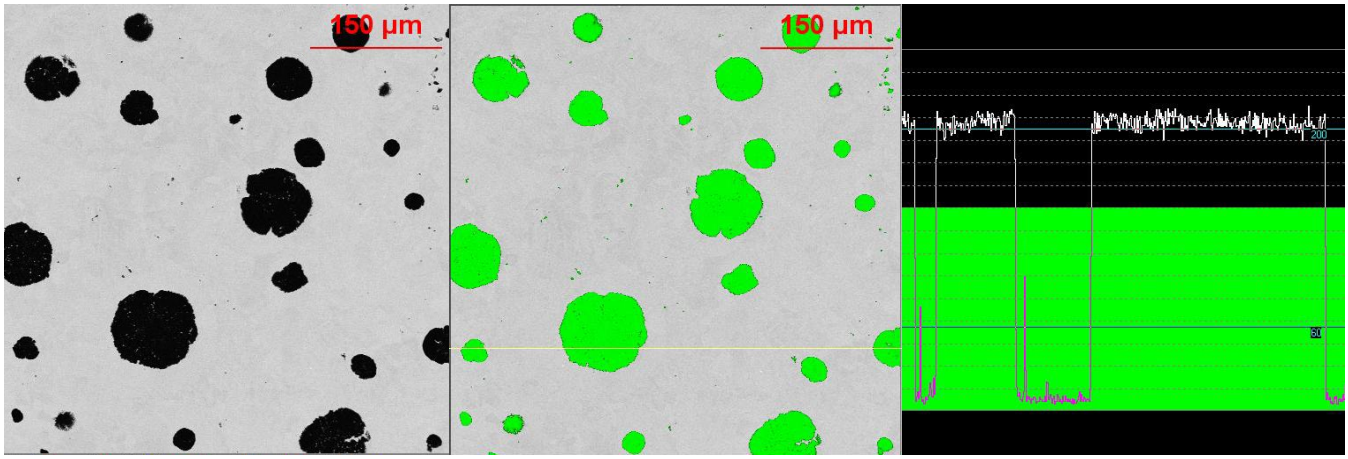

Figure 3. The SEM backscattered image provides optical contrast related to atomic number (light elements such as carbon are darker than heavy elements such as the Fe matrix, (b) thresholding phases of interests (green included, graphite, inclusions and micropores) and (c) upper/lower threshold setting using line scan). Particles in green indicate the ability to be detected by software.

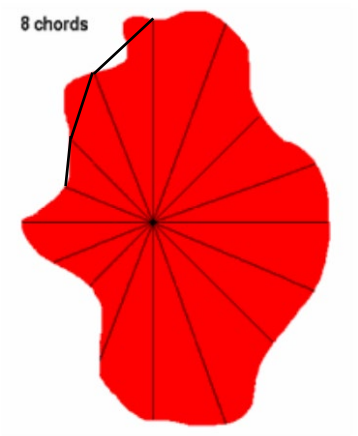

Figure 4. Eight chord raster used to determine the perimeter from the sum of connected chords ends.

For the most common graphite shapes in SGI and compacted graphite iron (CGI), the 8-chords close replicated a typical scale of convex and concave distortions and most importantly that this method is significantly less sensitive to a pixel/dimension ratio and orientation. Also, the sum of segments, which is calculated from the XY coordinates of the chord ends, has less integrated error when compared to measuring pixel by pixel the whole perimeter with boundary uncertainty.

The special automated algorithm was used to classify structural features based on the EDX spectrum using binary logic rules. The optimal sequence of classification rules was determined from several experimental trials (Fig. 6) and included the following classifications:

- Artifacts (pores):
  - (Al+Ca+Mn+Si+Mg+Ti+La+Ce+S)<6 and (Fe+O)>70at.%
- Graphite:
  - C>30at.%
- Inclusions and other:
  - True

Inclusions were identified by the total of the primary inclusion-forming elements, such as Al, S, Mg, Ca, Ti, Mn, Si, La, and Ce. If the total of these elements was greater than 6 at.%, the feature was classified as an inclusion. Any feature in which the sum of Fe and O was greater than 70 at.% was classified as an artifact, typically porosity or a polishing defect. This meant that the electron beam from EDS was capable of penetrating through the feature and detecting primarily the Fe matrix, thus not primarily carbon or inclusion elements. Any feature not meeting the previous criteria and containing greater than 30 at.% C was classified as graphite. These values were selected by point-by-point analysis of different micro-structural features in SGI.

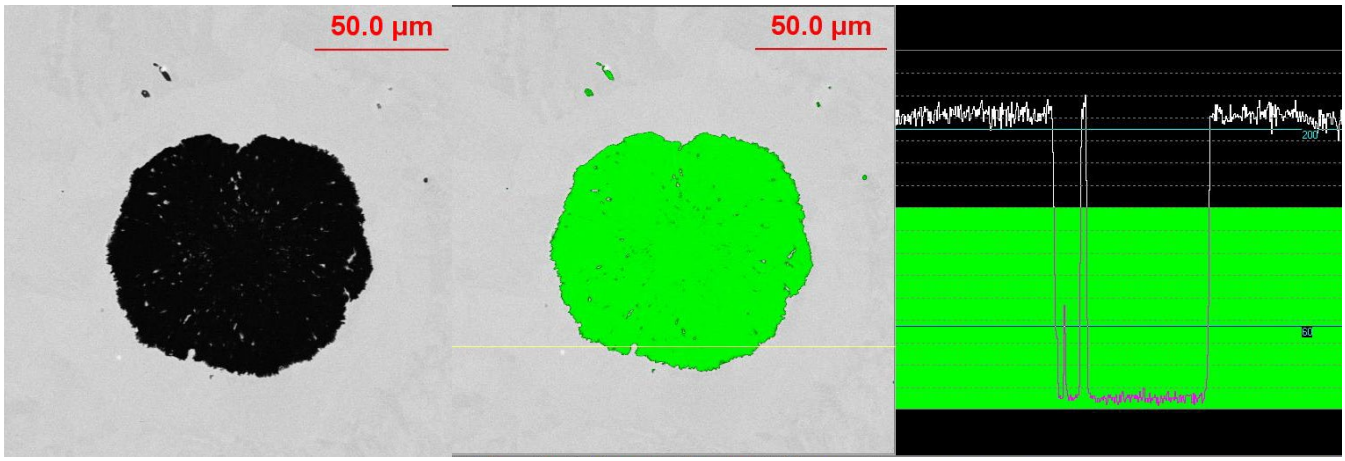

Figure 5. After detecting the particle of interest, the SEM automatically changed to high magnification (compared to Fig. 4a) and measured area by pixel number and perimeter using connected ends of 8 chord raster (Fig. 3).

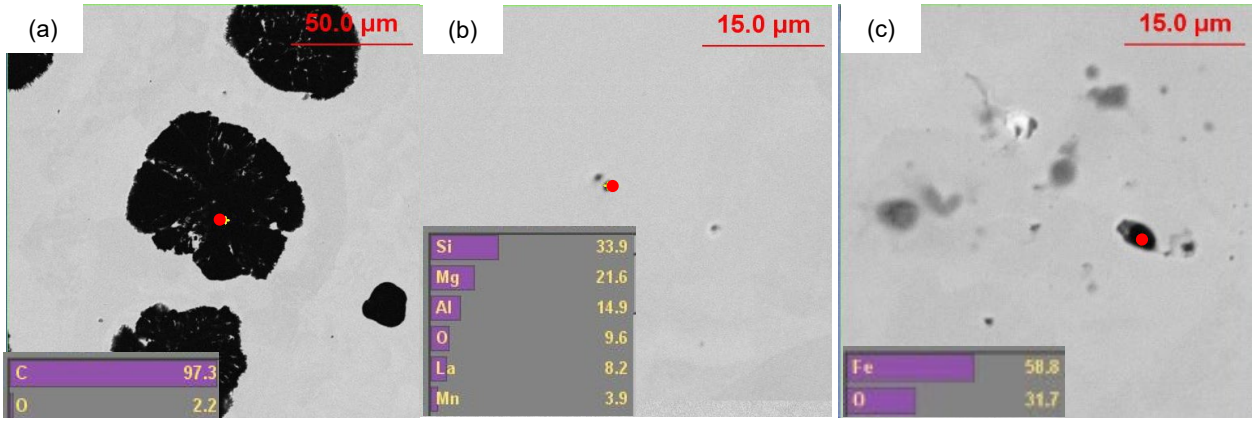

Figure 6. Example of the EDX spectrum from different features in SGI which was used to classify: (a) graphite, (b) non-metallic inclusions, and (c) micro-pores.

The examples of collected chemistry statistics for classified features in one SGI specimen are shown in Fig. 7 and indicated that applied rules were allowed to designate different microstructural features by EDX analysis. Figure 8 illustrates distribution of measured features in SGI by diameter. Such analysis is not possible for optical imaging which provided distorted statistics for micron sized features.

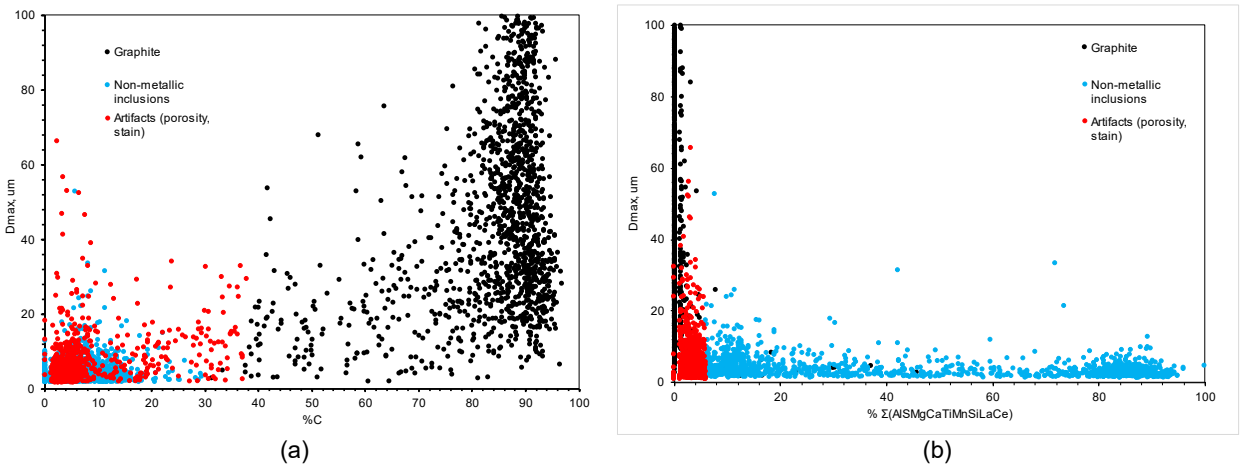

Figure 7. Example of EDX detected element concentrations in different microstructural features used in rule file for its classification: (a) graphite, (b) non-metallic inclusion. [View (c) shown on next page.]

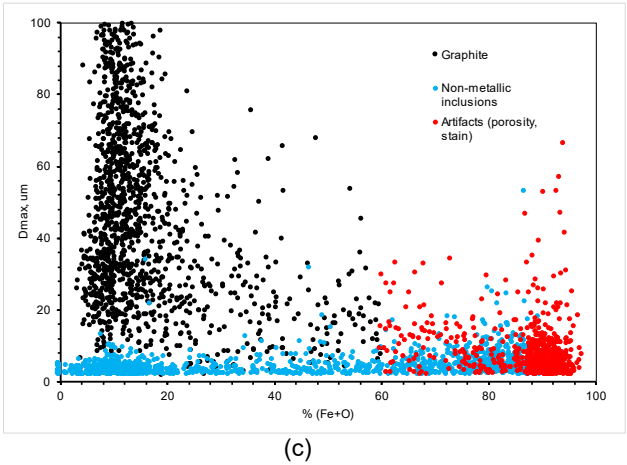

Figure 7. cont'd. Example of EDX detected element concentrations in different microstructural features used in rule file for its classification: (c) artifacts (porosity, stain) [views (a & b) shown on previous page].

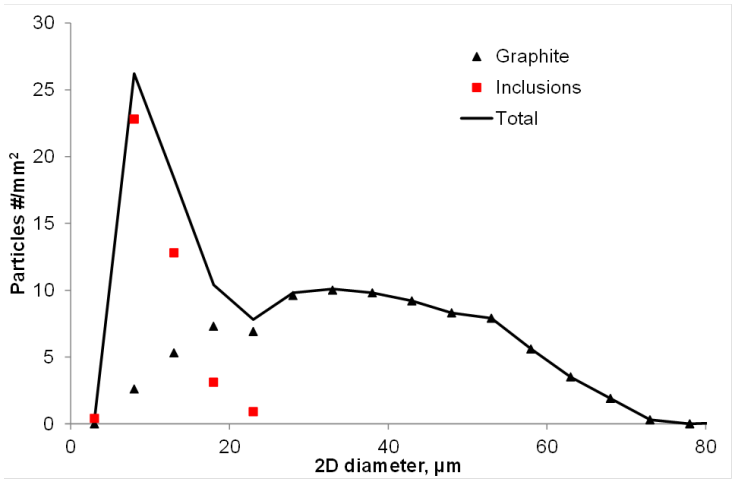

Figure 8. Example of determined by backscattered SEM image contrast total features number per unit area in SGI (solid black line -Total) and reclassified by EDS analysis these features on graphite and non-metallic inclusions.

To determine the effect of feature dimensions on the calculated shape factors, the special micro-lithography pattern with different diameter of circles from 1 to 100 micron was used (Fig. 9a). In theory, all measured shape factors needed to be equal unity. However, the statistical data indicated that a significant distortion was observed when feature diameter was close to settled resolution limit; therefore a 2 microns limit was used in this study. At the same time, the shape factor based on 8 chords perimeter (SSF1) was more realistic and closer to unity (Fig. 9c) when compared to the RSF shape factor determined from Feret diameter (Fig. 9b).

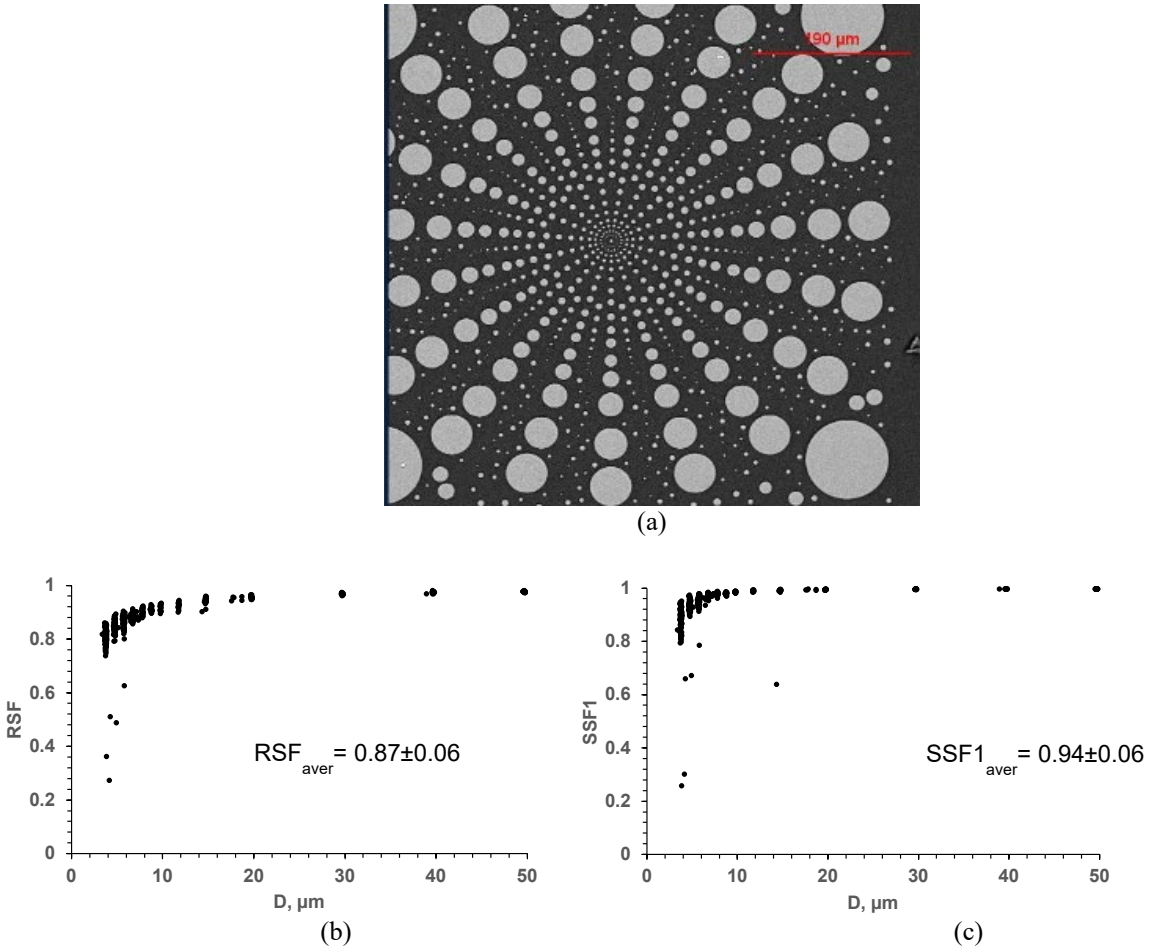

Figure 9. Pattern with ideal rounds of different diameters (a), shape statistics using two methods: RSF from Feret diameter (b), and perimeter from 8 chord raster method (c).

RESULTS

Contamination of boron and different levels of magnesium and other alloying elements may affect graphite nodularity. Three ductile irons with intentionally added different boron concentrations and that contained slightly different magnesium levels were used in this study (Table 2). All castings were poured from the same melt within a 150 second total timespan to reduce magnesium fade. These three ductile irons had 3.46±0.08 wt.% *C* and 2.64±0.06 wt.% Si. Chemistry was determined by optical emission arc spectroscopy and combustion analysis for carbon and sulfur. As shown in Table 2, the SGI had 27, 39 and 95 ppm boron, and magnesium levels varied from 280, 270, and 240ppm. The specimens for graphite shape analysis were extracted from step blocks that were cast in no-bake sand molds with 5 and 30 mm wall thicknesses. The lower threshold of ImageJ was 4 µm^2 and an appropriate equivalent diameter for AFA analysis was deemed to be 2µm.

Table 2. Chemistry of Studied SGI

SGI.	B (ppm)	Mg (ppm)
A	27±2	280±10
B	39±2	270±15
C	95±4	240±6

Optical metallography (Fig. 10) displays the visual increase in nodule size and nodule count as section size increases.

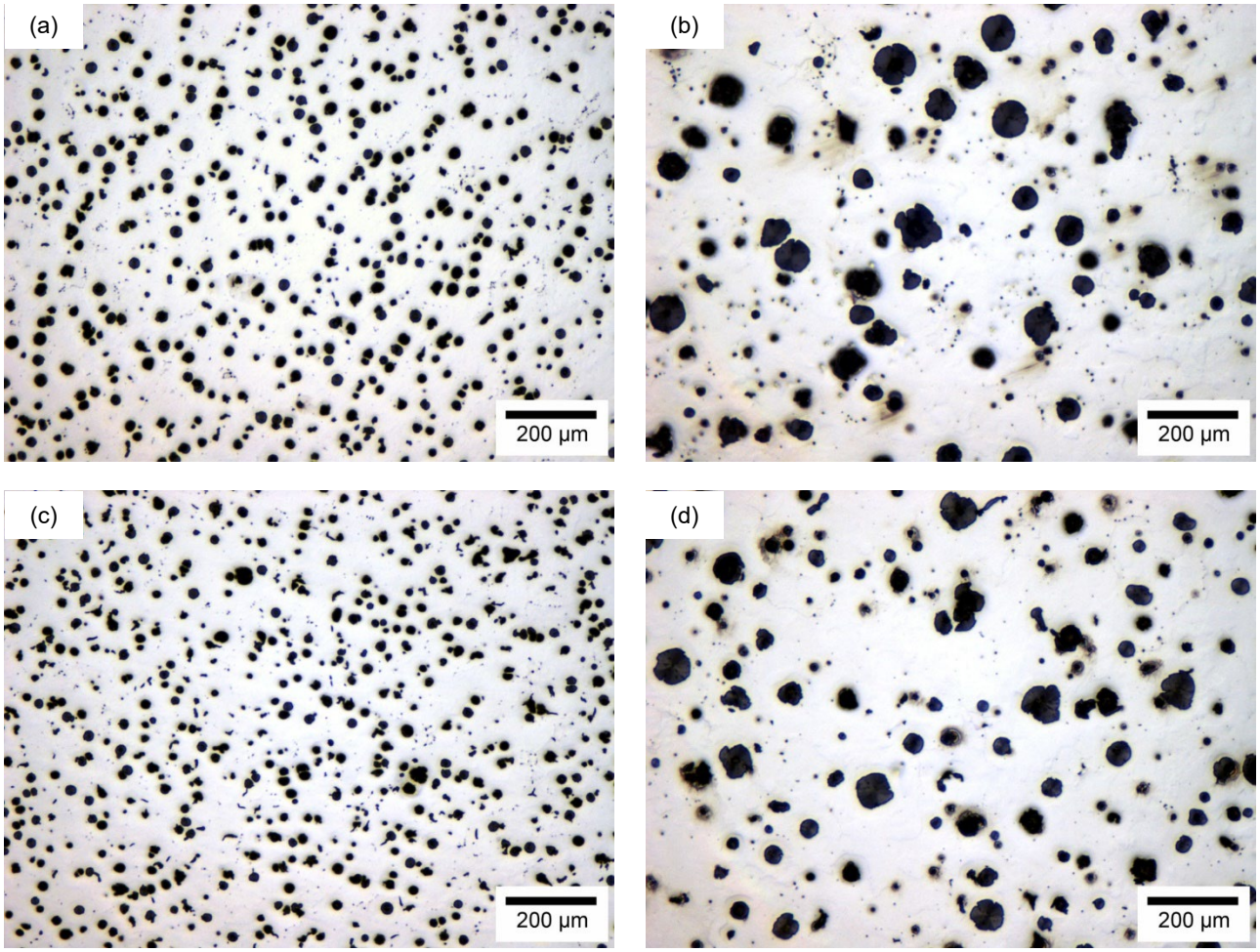

Figure 10. Optical images of microstructure of unetched SGI: (a) 27 ppm B 5 mm section, (b) 27 ppm B 30mm section, (c) 95 ppm B 5 mm section, and (d) 95 ppm B 30 mm section.

The results of graphite nodules quantification using an automated SEM/EDX analysis are shown in Fig. 11. More size distributions of graphite nodules are present in the larger step sizes. Smaller section sizes are prone to higher concentrations of smaller diameter graphite nodules.

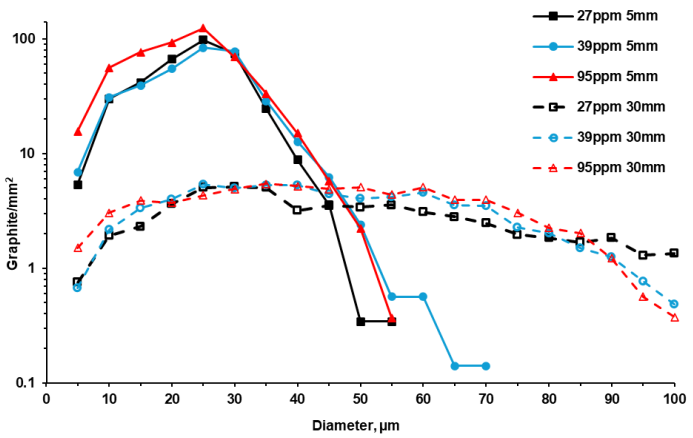

Figure 11. An automated SEM/EDX analysis of graphite nodule number distribution in studied SGI with different B contamination in 5 and 30 mm wall thicknesses.

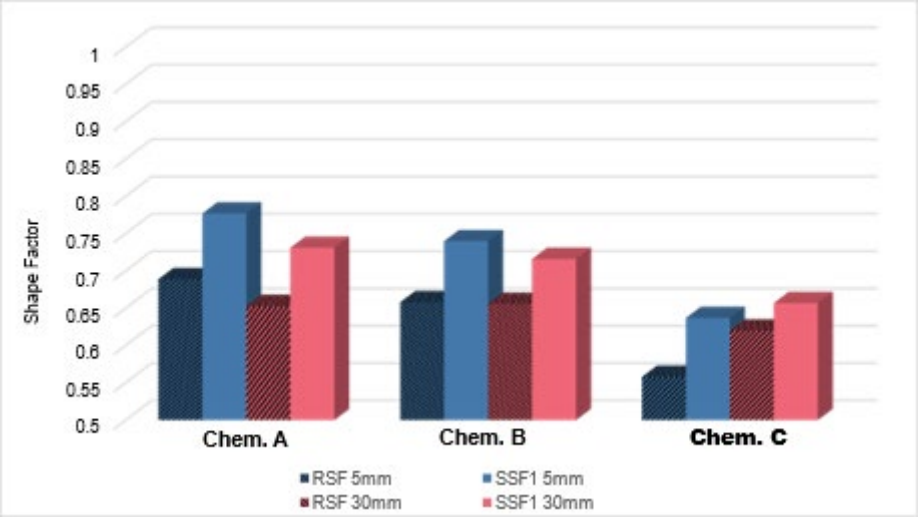

Figure 12. Two determined shape factors using Feret diameter (RSF) and perimeter from chord raster (SSF1) from the automated SEM/EDX method for study SGI in 5 and 30 mm wall thickness.

Figure 12 showed the effect of studied SGI chemistry on graphite nodules shape, as determined from Feret diameter (RSF) and by perimeters from 8 chords raster method (SSF1) suggested in this study. Both methods indicated that the nodularity was better in the thin 5mm section. Boron contamination appears to generally decrease nodularity slightly for consistent Mg contents around 270 ppm. At slightly faded levels of 240 ppm Mg, and as boron is increased to 95ppm, graphite nodule shape is further degraded. At the same time, a chord raster perimeter better reflects the measured graphite shape than shape calculated based on Feret diameter, as Feret diameter does not account for concavity of the graphite circumference.

DISCUSSION

The results of standard optical analysis using ImageJ software for shape quantification were compared with data obtained from suggested methodology (Fig. 13). The ideal pattern with circles of different diameters were used in both cases (Fig. 9a).

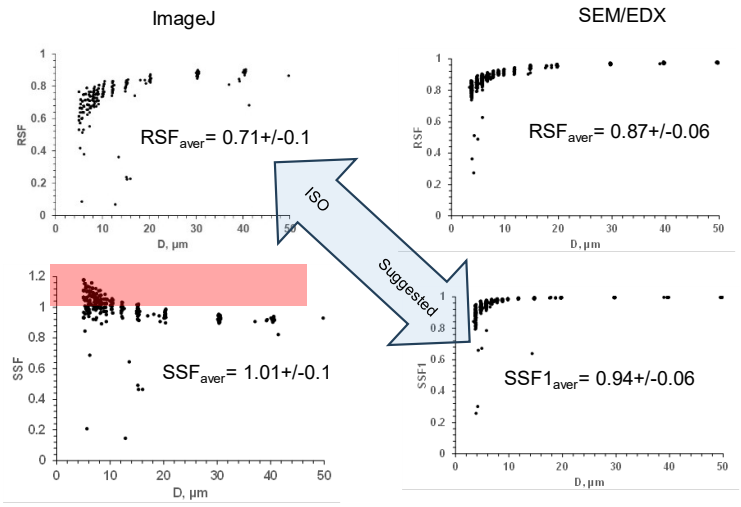

Figure 13. Comparison of shape factor statistics obtained from ideal rounds pattern (Fig. 8a) using ImageJ and automated SEM/EDX method using Feret diameter (RSF) and perimeter (SSF).

Two major disadvantages of optical analysis of standard ideal shape pattern were statistically proved:

- standard *RSF* method based on Feret diameter underestimated the shape factor of small particles (see top left graph in Fig. 13),
- at the same time, unrealistic values above unity were indicated using measured perimeter for calculating SSF shape factor because of the low accuracy of integrated perimeter.

The suggested SEM analysis based on 8 chord raster (SSF1) is less sensitive to small circular diameter and provided more realistic average results (see right lower graph in Fig. 13). Figure 14 illustrates graphite shape factors in studied SGI obtained from optical analysis. First, there is a large difference between two applied parameters. The RSF factor, based on Feret diameter, underestimated nodule shape and was not sensitive to structure differences in SGI A, B, and C. At the same time, SSF factor from measured perimeter showed unrealistic average large value near unity and even indicated improvement in graphite shape in heavy section in SGI. These results are supported by data obtained from counting ideal shape using pattern (Fig. 13).

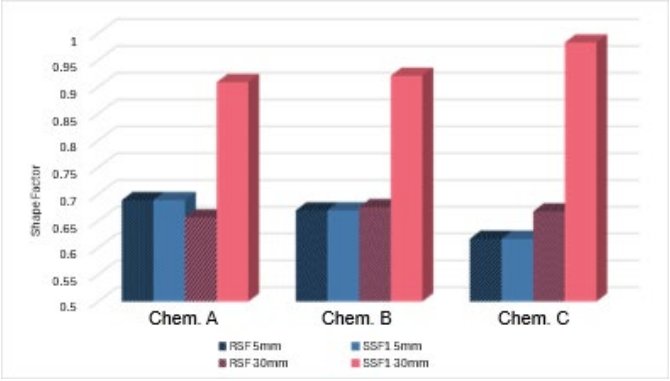

Figure 14. Shape factor of SGI with different boron in 5 and 30 mm step sizes determined by using ImageJ optical image analysis.

Figure 15 depicts the comparison of the calculated nodularity based on ISO 945 rule counting ratio of nodule areas above 0.6 nodularity to total nodule area. In the case of the standard optical imaging analysis, the shape factor based on Feret diameter (RSF) was used. These results were compared to the data obtained from automated SEM/EDX analysis, which: (i) separated graphite nodules from other features and (ii) used the perimeter from 8 chord raster to measure SSF1. Significant differences were observed in the determined nodularity obtained from

these methods. The suggested method provided more realistic, and the large values of calculated nodularity for each specific case with less variation. The suggested method also allowed determining the effect of contamination on graphite nodularity at different cooling rates, while standard analysis based on ISO 945 showed unclear results. Contamination of B and decrease of Mg level, distorted measured graphite nodularity in fast cooling castings while has a minor effect in slower cooling in 30 mm castings. It could also result from sensitivity of measurements result to dispersity of graphite nodules.

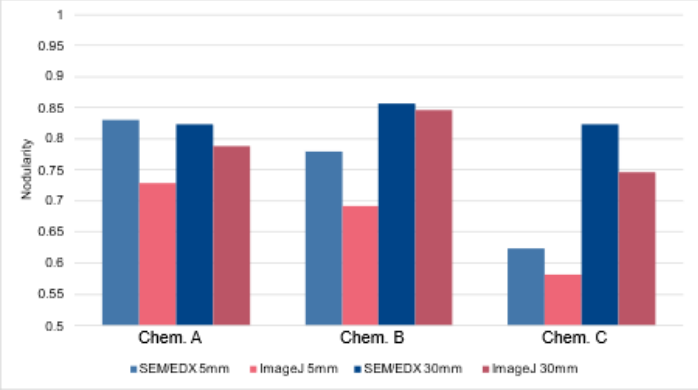

Figure 15. Determined graphite nodularity accordingly ISO recommendations for shape factor > 0.6 using data from standard optical ImageJ method (SSF1 from Feret diameter) and suggested automated SEM/EDX method (RSF1 – perimeter from 8 chord raster) for study SGI in 5 and 30 mm wall thicknesses.

Although the primary focus of this study was to develop and compare a new technique for more accurate analysis of graphite, it is interesting to note the potential effect of boron on degradation of nodule morphology. Unfortunately, the slightly decreasing Mg levels, from 280 to 240 ppm Mg, in this study obscured the effect of boron on graphite morphology. However, others have noted that boron has been observed to alter the surface morphology, increasing the surface roughness, of graphite spheres in levels as low as 24ppm while levels as high as 300 ppm can produce a noted decrease in nodularity.[20, 21] Boron is a surface active element and has been suggested to substitute for C atoms in the graphite lattice. A recent study by Muhammad et al. used various techniques to study the effect of trace elements, including boron, on the morphology of graphite in cast iron. It was shown by atomistic simulations that the B-C bond length in graphite is much shorter than the C-C bond which was suggested to cause strain in the lattice and curvature of the basal plane, resulting in boron favoring the flake morphology of graphite over spheroidal growth.[22] These results are interesting and further studies are planned by the authors to further illuminate the effects of boron in SGI with more consistent Mg levels.

CONCLUSION

A novel method for qualitative separation of different microstructural features and precise determination of its shape in cast iron was developed. A statistical comparison to standard optical imaging analysis was done using a micropattern with ideal shapes of different sizes and several SGI. It was proven that the 8 chord raster together with an advanced automated SEM/EDX analysis allowed the ability to separate graphite nodules from the other microstructural features and more realistically measure graphite nodule shape. This new method was applied to verify the combined effect of boron contamination and magnesium fade graphite nodule shape in different section size castings.

REFERENCES

1. Grenier, S., Labrecque, C., Bhattacharjee, A. *et al.* Inter-Laboratory Study of Nodularity and Nodule Count of Ductile Iron by Image Analysis. *Inter Metalcast* **8**, 51–63 (2014). https://doi.org/10.1007/BF03355582 (Link last accessed 03-31-2025.)
2. E. Wyatt and K. Holmes, "A Literature Survey Of The Effects of Certain Minor Elements On The Properties Of Nodular Iron," Army Materials and Mechanics Research Center, AMMRS MS 68-07, Watertown Arsenal, Watertown, Mass (1968).
3. Ductile Iron Data for Design Engineers, published by Rio Tinto Iron (1990).
4. Z. Wang, et al., “Effect of shrinkage porosity on mechanical properties of ferritic ductile iron,” China Foundry, 10(3), 141 (2013).
5. A. Solva, “The effects of non-metallic inclusions on properties relevant to the performance of steel in structural and mechanical applications,” *Journal of*

Materials Research and Technology, 8 (2) 2408 (2019).
6. S. Lekakh, J. Qing, "Engineering Heterogeneous Nucleation during Solidification of Multiphase Cast Alloys: An Overview," *Metals*, 13, 1154, 1 (2023).
7. Lekakh, S.N. Searching for Graphite Nodule Nuclei Using Automated SEM/EDX Analysis. *Inter Metalcast* 14, 1078–1089 (2020). https://doi.org/10.1007/s40962-020-00418-1 (Link last accessed 03-31-2025.)
8. D. Stefanescu et al., "Growth of spheroidal graphite on nitride nuclei: disregistry and crystallinity during early growth," *Metall. Mater. Trans. A*, 50 (4)1763 (2019).
9. J. Sertucha, J. Lacaze, "Casting Defects in Sand-Mold Cast Irons—An Illustrated Review with Emphasis on Spheroidal Graphite Cast Irons," *Metals* 12(3), 504 (2022).
10. A. De Santis et al., "Quantitative Shape Evaluation of Graphite Particles in Ductile Iron, *Journal of Materials Processing Technology*, 196 (1–3) 292 (2008).
11. D. Anca, et al., "Graphite Compactness Degree and Nodularity of High-Si Ductile Iron Produced via Permanent Mold versus Sand Mold Casting," *Materials* (Basel), 15 (8) 2712 (2022).
12. Lekakh, S., Zhang, X., Tucker, W., Lee, H., Selly, T., Schiffbauer, J., "3D Characterization of Structure and Micro-porosity in Two Cast Irons with Spheroidal Graphite," *Materials Characterization*, 158, 109991 (2019).
13. ISO 1083:2018, Spheroidal graphite cast irons — Classification. (Link last accessed 02-17-2025.) https://www.iso.org/standard/66643.html
14. Y. Takashimizu and M. Iiyoshi, "New parameter of roundness R: circularity corrected by aspect ratio," *Progress in Earth and Planetary Science*, 3:2 (2016).
15. I. Riposan et al., "Graphite Nodularity Evaluation in High-Si Ductile Cast Irons," *Materials*, 15, 7685 (2022).
16. A. Gadek-Moszczak, "The impact of the resolution of the measured object on the assessment of its perimeter," *Production Engineering Archives*, 25, 47-51 (2019).
17. ImageJ software, https://www.smartdeploy.com/ (Link last accessed 02-17-2025.)
18. Lehrer, C., Bartlett, L., Lekakh, S., Schroeder, C., "Understanding the Effect of Boron on the Microstructure and Mechanical Properties of Pearlitic Ductile Irons," 2025 *AFS Metalcasting Conference Proceedings*, Paper #25-089 (2025).
19. Harris, M., Adaba O., Lekakh, S., O'Malley R., Richards, V., "Improved Methodology for Automated SEM/EDS Non-Metallic Inclusion Analysis of Mini-Mill and Foundry Steels," *AISTech Proceedings,* pp. 3315-3325 (2015).
20. Bugten, A.V., Michels, L., Brurok, R.B. et al., "The Role of Boron in Low Copper Spheroidal Graphite Irons," *Metall Mater Trans A,* 54, 2539–2553 (2023). https://doi.org/10.1007/s11661-023-07014-y (Link last accessed 03-31-2025.)
21. Zou, Y., Ogawa, M. and Nakae, H., "Interaction of boron with copper and its influence on matrix of spheroidal graphite cast iron," ISIJ International, Vol. 52, No. 3, 2012 pp. 505-509.
22. Muhammad, H. and Fredriksson, H., "Relationship between the trace elements and graphite morphologies in cast iron," Met. Trans A. Vol 45A 2014, p. 6187.